processes

MDPI

Article

Mechanical and Shrinkage Properties of Alkali-Activated Binder-Stabilized Expansive Soils

Yongke Wei [1,2], Weibo Tan [3], Jiann-Wen Woody Ju [4], Yinghui Tian [5], Shouzhong Feng [3,*], Changbai Wang [3], Qiang Wang [3] and Peiyuan Chen [3]

[1] College of Civil Engineering, Tongji University, Shanghai 200092, China
[2] Guangxi Transportation Design Group Co., Ltd., Nanning 530029, China
[3] School of Civil Engineering and Architecture, Anhui University of Science and Technology, Huainan 232001, China
[4] Department of Civil and Environmental Engineering, University of California, Los Angeles, CA 95616, USA
[5] Department of Infrastructure Engineering, Faculty of Engineering and Information Technology, The University of Melbourne, Parkville, VIC 3010, Australia
* Correspondence: fsz63@vip.163.com

Abstract

Expansive soil is prone to significant swelling and shrinkage deformation with changes in moisture conditions, posing serious safety hazards to engineering construction. This study focuses on alkali-activated self-compacting fluid-solidified soil (ASFS) and systematically explores the regulatory effect of expansive soil with different dosages (0–100%) on its properties. This study analyzes the influence of expansive soil on the setting time, hydration characteristics, autogenous shrinkage, and compressive strength of ASFS while verifying the feasibility of this method for solidifying expansive soil through microstructural analysis. The results show that, with the increase in content of expansive soil, the initial and final setting times of ASFS were prolonged by 0.08–1.58 times and 0.08–1.29 times, respectively. Although expansive soil inhibited the hydration of ASFS, it could compensate for autogenous shrinkage through the expansion effect of clay minerals, reducing the autogenous shrinkage by 13.4–51.2%. Furthermore, the optimal dosage of expansive soil in ASFS is 60%. Compared with the control group, the 7d compressive strength of ASFS increases by 52.4%, the strength after 3d water immersion rises by 62.6%, and the strength after eight wet–dry cycles still remains 10% higher. This optimal dosage achieves the best balance between mechanical properties, water stability, and shrinkage resistance of ASFS, providing a reliable technical reference for the efficient utilization of expansive soil in engineering.

Keywords: alkali-activated; expansive soil; compressive strength; autogenous shrinkage; hydration

Check for updates

Academic Editor: Jacopo Donnini

Received: 9 November 2025
Revised: 6 December 2025
Accepted: 17 December 2025
Published: 19 December 2025

Copyright: © 2025 by the authors. Licensee MDPI, Basel, Switzerland. This article is an open access article distributed under the terms and conditions of the Creative Commons Attribution (CC BY) license.

1. Introduction

Expansive soil is a type of highly plastic clay, which mainly contains hydrophilic minerals such as montmorillonite and illite in its composition. Among these minerals, montmorillonite exhibits extremely high sensitivity to water and shows greater swelling potential when the water content increases [1,2]. In addition, the water inside expansive soil tends to exhibit uneven distribution, which leads to obvious differences in the swelling and shrinkage rates of different parts of the soil mass, further resulting in irregular cracks [3,4]. As water is repeatedly lost, the soil structure will eventually undergo instability and damage [5]. Consequently, expansive soil is prone to causing various serious problems

in engineering practice, such as dyke seepage, road cracking, and building foundation instability [6]. This not only significantly increases the later maintenance costs of the project but also may induce safety risks, posing a serious threat to the stable operation of transportation, water conservancy, and construction projects. Therefore, targeted treatment of expansive soil is of crucial necessity for reducing risks in engineering construction and application [7].

A common method for treating expansive soil in construction engineering is to use lime and cement for modification [8–11]. As cementitious materials, lime and cement form a dense matrix in the expansive soil through hydration reactions, thereby improving the strength and durability of expansive soil. For instance, Ako et al. [8] investigated the effect of cement with different dosages on the mechanical properties of expansive soil. The results showed that, when cement grout with quantities of 6% was injected, the soil swelling was reduced by 90%. Stoltz et al. [9] analyzed the effects of quicklime on the volumetric properties of expansive soil. They found that quicklime could inhibit the swelling potential of expansive soil and, with its dosage over 5%, enhance the stress sensitivity of expansive soil. However, the production process of these two materials not only consumes a large amount of energy but also emits carbon dioxide, sulfur dioxide, and other dust, exerting adverse impacts on the environment [12,13]. Therefore, it is of great significance to find a cementitious material that combines a good modification effect with green and environmentally friendly properties.

Alkali-activated slag materials (AAS) can effectively replace cement and lime for expansive soil solidification. Compared with cement and lime, AAS is mainly made from slag, an industrial by-product, which can significantly reduce carbon dioxide emissions [14–16]. Existing studies have shown that the C-(A)-S-H gel generated by AAS can form a dense internal structure with soil particles, thereby enhancing the compressive strength of the soil [17–19]. For example, Yi et al. [20] compared the stabilization effects of AAS (prepared with different activators) and cement on soil. They indicated that, when NaOH was used as the activator, the compressive strength of AAS solidified soil was higher than that of cement solidified soil after 28 and 90 days of curing. However, current relevant studies mostly focus on the fundamental characteristics of AAS solidified soil under conventional conditions, while systematic research on the mechanical properties of expansive soil in AAS solidified soil under the self-compacting fluid state is still relatively scarce.

Based on this, this study aims to investigate the mechanical and shrinkage properties of alkali-activated self-compacting fluid-solidified soil (ASFS). Unlike traditional approaches that treat expansive soil merely as "problematic soil" requiring modification to mitigate its swelling risks, this study innovatively reclassifies expansive soil as an "engineered additive" for the ASFS system. It leverages its clay mineral expansion characteristics to directly compensate for autogenous shrinkage of ASFS, thereby realizing a "problem-to-solution" transformation. Specifically, this study explores the influence patterns of different expansive soil dosages on the fluidity, hydration reactions, and hydration products of ASFS. In addition, SEM, MIP and TGA were used to analyze the microstructure of ASFS. This study is of great significance for advancing the technical theory of AAS solidified soil and broadening its engineering utilization in regions with expansive soil.

2. Materials and Methods

2.1. Raw Materials

Grade S105 slag was sourced from Lingshou County Jixi Mineral Products Co., Ltd., Shijiazhuang, China. Expansive soil was sampled from the Nanning Highway in Guangxi Zhuang Autonomous Region, Nanning, China. The specific surface areas of the two materials are 360 m^2/kg and 240 m^2/kg, respectively. Their chemical compositions were

analyzed by RIGAKU ZSX Primus X-ray fluorescence spectroscopy (Rigaku Corporation, Tokyo, Japan), with the results presented in Table 1. Figure 1 shows the particle size distribution curves of the slag and expansive soil. Figure 2 presents the photograph and morphology of expansive soil. In addition, the expansive soil has a liquid limit of 33.6%, a plasticity index of 16%, a specific gravity of 2.7, and a free swell potential of 41%. The quartz powder has a particle size range of 120–180 μm. In addition, the CP-1200 water reducing agent was supplied by Nanjing Xinyi Synthetic Technology Co., Ltd., Nanjing, China. Water glass and NaOH were sourced from Sinopharm Chemical Reagent Co., Ltd., Shanghai, China.

Table 1. Chemical compositions of GGBFS and Expansive soils (%).

	SiO_2	Al_2O_3	Fe_2O_3	K_2O	TiO_2	MgO	CaO	Others
Expansive soils	82.63	11.04	2.96	1.48	1.15	0.33	0.15	0.26
Slag	27.2	18.2	0.4	0.4	-	7.8	45.2	0.8

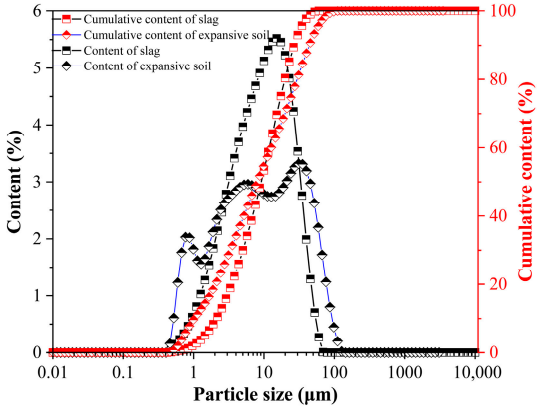

Figure 1. Particle size distribution profiles of slag and expansive soil.

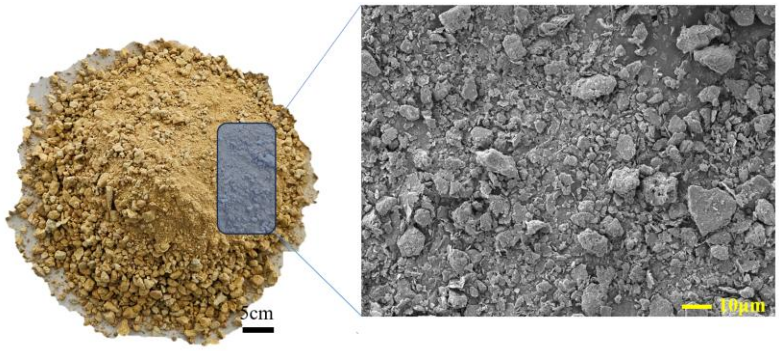

Figure 2. Photograph and morphology of expansive soils.

2.2. Mix Proportion and Samples

Table 2 lists the mix proportions of ASFS. For the blank ASFS, E0Q10, the alkaline equivalent was 5% and the activator modulus was set to 1.0. An equal-mass replacement strategy was adopted in this study, where quartz powder was substituted with expansive soil at different proportions to investigate the influence of expansive soil content on the properties of ASFS.

Table 2. Proportion of pastes (100 g).

Groups	Expansive Soils	Quartz Powder	Slag	Superplasticizer	NaOH	Water Glass	Water
E0Q10	0	49.83	19.93	0.35	3.15	12.53	14.32
E2Q8	9.96	39.86	19.93	0.35	3.15	12.53	14.32
E4Q6	19.63	29.90	19.93	0.35	3.15	12.53	14.32
E6Q4	29.90	19.63	19.93	0.35	3.15	12.53	14.32
E8Q2	39.86	9.96	19.93	0.35	3.15	12.53	14.32

The preparation procedure of the activator solution was carried out as follows. First, NaOH was added to water and stirred until dissolved. After the solution was naturally cooled to room temperature, water glass was added according to the proportion in Table 2, followed by continuous stirring until completely dissolved, and then the solution was left to stand for later use. In addition, dissolve CP-1200 in activator in advance, stir evenly and ensure it is fully dissolved. For the mixing process of ASFS, slag, expansive soil, and quartz powder were first dry-blended for 3 min. The prepared activator solution was then added to the dry mixture, followed by further stirring for another 3 min.

2.3. Testing Methods of Samples

2.3.1. Setting Times

The setting times of ASFS were measured using a Vicat needle by ASTM C191 [21], and the measurement was conducted in the standard curing room at 20 ± 3 °C and RH ≥95%.

2.3.2. Fluidity

The fluidity of ASFS was tested by an STNLD-3 jump table according to ASTM C1437 [22]. The mean spread along two orthogonal directions was reported. In addition, the fluidity of the self-compacting fluid must meet the 200 mm requirement specified in ASTM C476 [23].

2.3.3. Hydration Kinetics

The hydration kinetics of ASFS were analyzed using isothermal calorimetry as specified in ASTM C1702 [24]. A 50 g mixed paste sample was positioned in a glass container and inserted into the calorimeter to gather the heat it emitted over 72 h. Before measurement, the calorimeter underwent calibration at 25 °C.

2.3.4. Autogenous Shrinkage

In accordance with ASTM C1698, the autogenous shrinkage of ASFS was determined by the corrugated tube method [25]. In this experiment, corrugated polyethylene (PE) molds with a length of 420 mm and a diameter of 29 mm were used. The samples were then sealed and horizontally placed on corrugated plates in a standard curing room at 20 ± 3 °C and RH ≥95%. One end of the sample was fixed on the test bench, and the other end was in contact with a digital micrometer to measure the length change in autogenous shrinkage after final setting time [26]. The length changes in the sample were recorded by a digital dial gauge with an interval of 10 min for 7 days.

2.3.5. Hydration Products Analysis

To identify the hydration products of AAS paste, a Rigaku Smartlab (Rigaku Corporation, Tokyo, Japan) X-ray diffractometer (XRD) was utilized. To prepare the samples, hydration was terminated first, followed by grinding into powder. The scanning speed was 2°/min. This study employed a STA 449 F3 Jupiter (NETZSCH-Gerätebau GmbH, Selb, Germany) thermogravimetric analyzer (TG) to conduct thermogravimetric loss tests.

The sample preparation was consistent with that described in Section 2.3.5. Subsequently, sample was heated from room temperature to 900 °C at a heating rate of 10 °C/min.

2.3.6. Compressive Strength

The compressive strength was assessed using specimens as specified in ASTM C192 [27]. ASFS was poured into cylindrical molds (Φ50 mm × 100 mm), cured in a conditioning room at 20 ± 3 °C and RH ≥95% for 7 days, and then 6 specimens were tested to calculate the average compressive strength and standard error.

Following initial testing, the specimens were immersed in water for 3 days, after which their compressive strength was measured again. Additional specimens were cured until 28 days of age for wet–dry cycle testing. Each cycle consisted of two stages: saturation by immersion in water for 24 h, followed by drying in an oven at 45 °C for 24 h. Mass and compressive strength were measured every two cycles. The test was terminated after eight complete cycles.

2.3.7. Microstructural Characterization

The pore structure of ASFS was tested using a MicroActive AutoPore V 9600 (Micromeritics Instrument Corporation, Norcross, GA, USA) MIP, with samples taken from the specimens used for 7d compressive strength testing. The microstructure of ASFS was characterized using a FlexSEM1000 SEM (HITACHI, Tokyo, Japan). Prior to testing, the sample was sputter-coated with gold to enhance its electrical conductivity.

3. Results

3.1. Setting Times

Figure 3 shows the setting time of ASFS. It can be seen that adding expansive soil significantly prolongs the setting time of ASFS. Compared to E0Q10 without expansive soil, the content of expansive soil has an obvious positive correlation with the setting time of ASFS. Specifically, when the content of expansive soil increases from 20% to 100%, the initial setting time of AASS was prolonged by 0.08–1.58 times, and the final setting time was prolonged by 0.08–1.29 times. This suggests that the addition of expansive soil can avoid the negative effects of rapid setting of ASFS. This retardation indicates that clay minerals in expansive soil adsorb alkaline substances required for hydration, reducing the alkaline concentration of the paste. And the hydration film formed by water absorption of expansive soil particles that induces a coating effect on the slag surface physically blocks the contact between the activator and slag particles and inhibits the early formation of C-(A)-S-H gel [28,29].

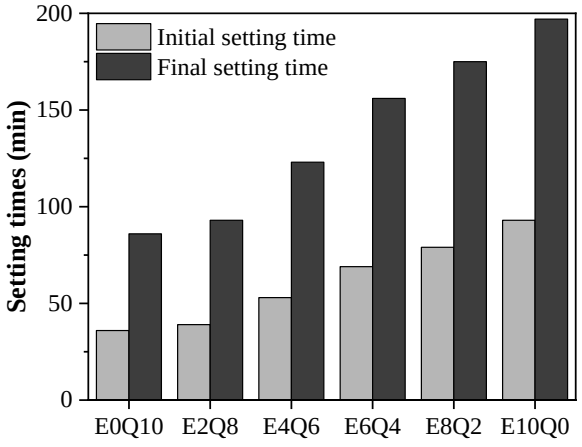

Figure 3. Setting times of ASFS.

3.2. Fluidity

Figure 4 presents the fluidity of ASFS. When no expansive soil was added, the fluidity of E0Q10 was 280 mm, which fully meets the requirement of a minimum fluidity of 200 mm for self-compacting mortar specified in ASTM C476. With the addition of expansive soil, the fluidity of ASFS showed a significant downward trend, and the degree of decrease was closely related to the content of expansive soil. Specifically, when the content of expansive soil was 20–60%, the fluidity decreased to 205–255 mm, which was 8.9%, 17.9%, and 26.8% lower than that of E0Q10, respectively. Despite this reduction, the fluidity of ASFS still met the basic requirements for self-compacting performance. This is because expansive soil, with strong water absorption, takes in much free water during ASFS mixing, reducing water for particle lubrication, increasing inter-particle friction, and thus greatly decreasing ASFS fluidity [30,31]. In addition, when the content of expansive soil was further increased to 80%, the fluidity of E8Q2 decreased to 195 mm, which is below the specification threshold of 200 mm. This indicates that high-content expansive soil will severely damage the self-compacting characteristics of ASFS, failing to meet the requirement of dense forming without vibration in engineering applications.

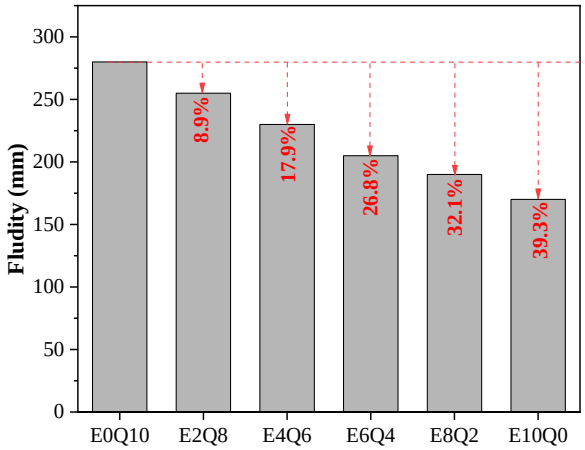

Figure 4. Fluidity of ASFS.

3.3. Hydration Kinetics

Figure 5 shows the hydration kinetics of ASFS with different contents of expansive soil. In Figure 5a, the first peak is a dissolution peak, which typically corresponds to the dissolution of slag and the formation of a small amount of hydration products [29]; the second peak is a bulk peak, primarily associated with the formation of hydration products, such as C-(A)-S-H gel [32].

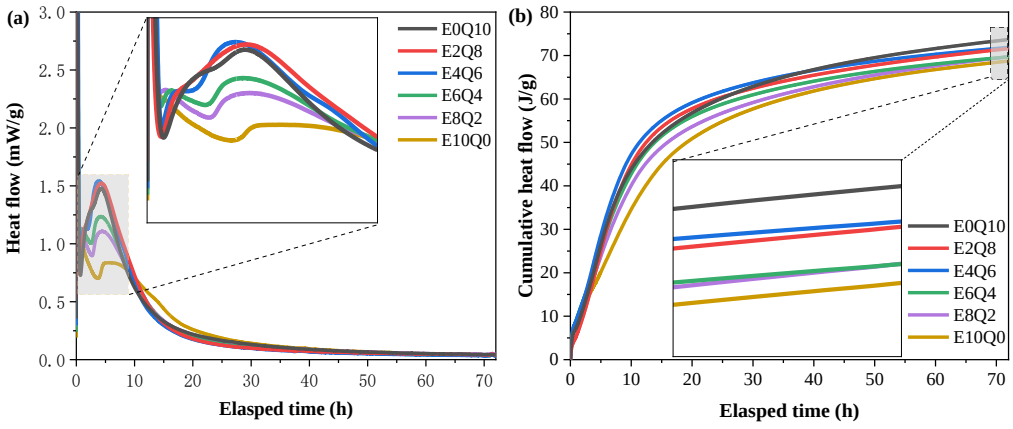

Figure 5. Hydration heat flow (**a**) and cumulative hydration heat (**b**) of ASFS.

The incorporation of expansive soil can inhibit the early-stage hydration process of ASFS. When the content of expansive soil was increased, the bulk peak of ASFS was decreased gradually. This indicates that expansive soil can reduce the heat release by regulating the hydration reaction path, and the decrease in heat release further slows down the kinetic rate of the early hydration reaction, ultimately forming a synergistic effect of "increased content—reduced heat release—hydration inhibition".

In addition, Figure 5b presents the cumulative hydration heat of ASFS. Compared with E0Q10, as the content of expansive soil increased, the total mass loss of ASFS decreased by 2.8–6.7%. This result is consistent with the test findings in Section 3.1 that expansive soil delays the setting time. Previous studies have shown that expansive soil has a high water absorption capacity, which reduces the effective w/b ratio of the paste and thereby inhibits the early hydration process of ASFS [33,34].

3.4. Autogenous Shrinkage

Figure 6 presents the autogenous shrinkage of ASFS. It can be seen that the autogenous shrinkage of E0Q10 developed rapidly, with the autogenous shrinkage strain reaching 2165.3 με at 7 days, indicating a significant increase in the cracking risk of ASFS.

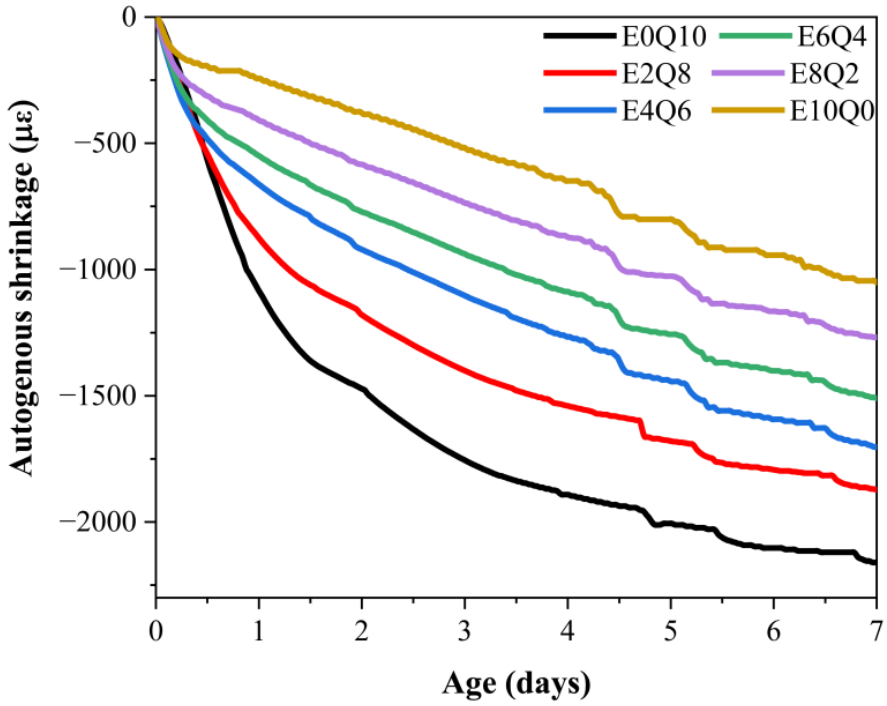

Figure 6. Autogenous shrinkage of ASFS over 7 days.

In contrast, the addition of expansive soil can mitigate the autogenous shrinkage of ASFS. To quantitatively reveal the correlation law between them, linear fitting analysis was performed based on the 7d autogenous shrinkage strain test data under different expansive soil contents, yielding the fitting equation $y = -(10.7 \pm 0.3)\,x + (2133.1 \pm 21.1)$ with a goodness of fit $R^2 = 0.99$. The high R^2 value indicates an extremely strong linear negative correlation between the expansive soil content and the 7d autogenous shrinkage of ASFS: for every 1% increase in the expansive soil content, the 7d autogenous shrinkage of ASFS decreases by an average of 10.7 με. For instance, when the content of expansive soil was increased from 20% to 100%, the autogenous shrinkage of ASFS was decreased by 13.4–51.2%. This suggests that replacing quartz powder with expansive soil can reduce the autogenous shrinkage of ASFS, thereby lowering its cracking risk. This shrinkage reduction

is attributed to the expansion of clay minerals (e.g., montmorillonite) in expansive soil during hydration, which in turn compensates for the autogenous shrinkage of ASFS [35].

3.5. XRD

Figure 7 shows the XRD patterns of ASFS. The main mineral phases in the samples were identified as quartz, gismondine, and C-A-S-H by comparing with the existing literature [36]. It should be noted that no gismondine phase was detected in E0Q10; nevertheless, by adding expansive soil, a gismondine phase was formed in ASFS, and the characteristic diffraction peak of this mineral phase overlapped partially with that of quartz. Specifically, an obvious characteristic diffraction peak of gismondine in ASFS with expansive soil can be observed at $2\theta = 26.6°$. This phenomenon is closely related to the clay minerals, which undergo structural breakdown in an alkaline environment and then participate in reactions to form gismondine [36].

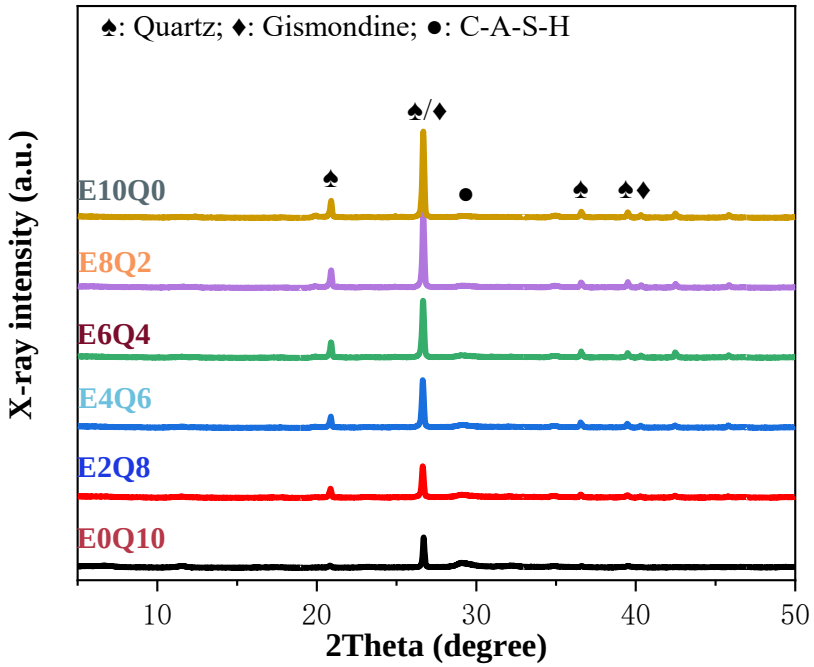

Figure 7. XRD patterns of ASFS at 7 days.

3.6. TG-DTG

Figure 8 shows the TG-DTG curves of ASFS. In the DTG curve, the mass loss in the temperature range of 30–200 °C mainly corresponds to the dehydration process of C-A-S-H gel [37,38]. When expansive soil was added, the peak value of the DTG curve of ASFS was decreased significantly compared with E0Q10. This indicates that the formation of hydration product of C-A-S-H is inhibited in ASFS with expansive soil. Furthermore, the total mass loss of the ASFS decreased with the increase in the content of expansive soil. For instance, when the content of expansive soil reached 100%, the total mass loss of E10Q0 was 54% lower than that of E0Q10. This indicates that expansive soil reduces the hydration degree of ASFS. This result is consistent with the hydration kinetics results, suggesting that expansive soil restricts the hydration reaction of slag, thereby reducing the formation of hydration products of ASFS [39].

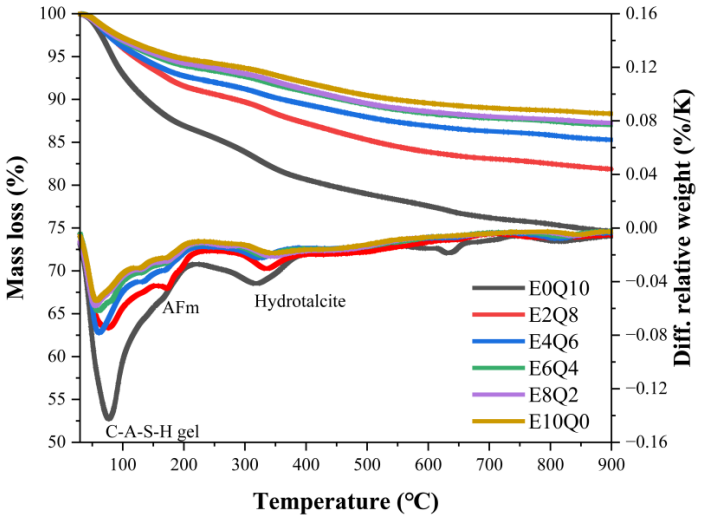

Figure 8. TG-DTG results of ASFS.

3.7. Compressive Strength

3.7.1. Compressive Strength for 7 Days

Figure 9 shows the compressive strength of ASFS. It is evident that incorporating expansive soil can enhance the compressive strength of ASFS, and this enhancement is associated with the dosage of expansive soil. When the content of expansive soil was raised from 20% to 60%, the compressive strength of ASFS increased by 33.6–52.4% in comparison to E0Q10. This indicates that the reasonable incorporation of expansive soil can optimize the mechanical properties of ASFS. This strength enhancement is associated with the hydration reaction of expansive soil. Its clay minerals participate in the reaction in an alkaline environment, and the generated hydration products optimize the microstructure, thereby contributing to the improvement of the compressive strength of ASFS [40,41]. Nevertheless, with further increase in the content of expansive soil, the compressive strength of ASFS decreased compared with E6Q4, while it was still higher than that of E0Q10. This is because the fine particles of expansive soil are prone to accumulation and congestion, leading to an imbalance in the packing of ASFS. Meanwhile, its strong water absorption characteristics significantly inhibit the hydration reaction kinetics, resulting in insufficient generation of hydration products and ultimately leading to a decrease in compressive strength of ASFS [42].

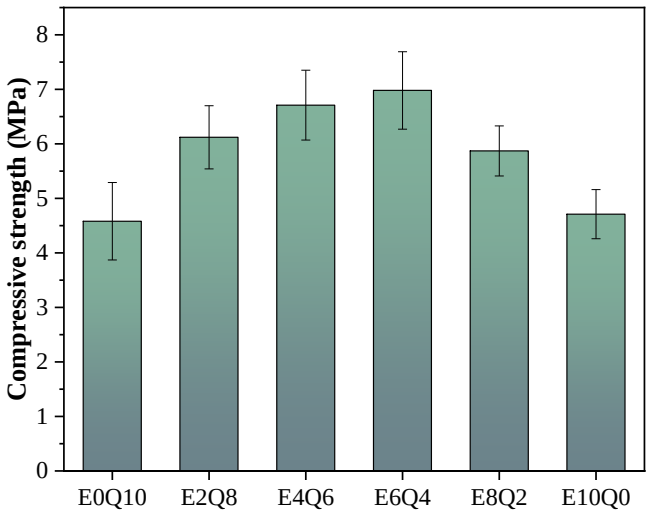

Figure 9. Compressive strength of ASFS at 7d.

3.7.2. Unconfined Compressive Strength for 10 Days

Figure 10 presents the compressive strength of ASFS. After 7 days of curing followed by 3 days of immersion, the compressive strength of ASFS with expansive soil was higher than that of E0Q10. When the content of expansive soil was 60%, the compressive strength of E6Q4 reached the maximum value, which was 62.6% higher than that of E0Q10. This indicates that the ASFS system can prevent the phenomenon where expansive soil causes a decrease in compressive strength due to swelling upon water contact. This strength improvement is attributed to the dense structure of hardened ASFS physically restricting expansive soil swelling, while its hydration products encapsulate expansive soil and reduce its hydrophilicity, thereby avoiding adverse effects on the compressive strength of ASFS [43].

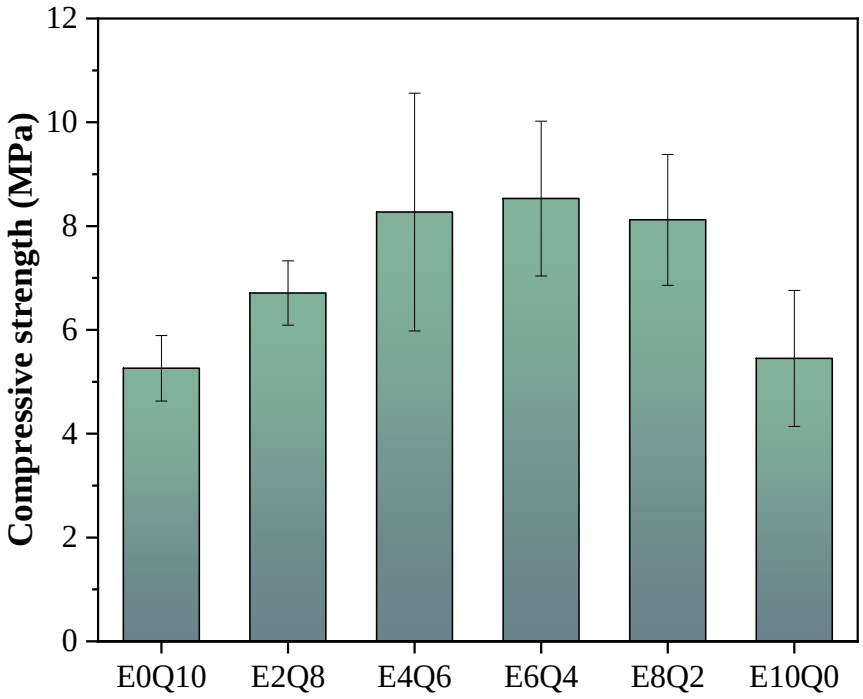

Figure 10. Compressive strength of ASFS after 7d curing and 3d immersion.

3.7.3. Unconfined Compressive Strength for Drying and Wetting Cycle

Figure 11 illustrates the compressive strength of ASFS under varying numbers of wet–dry cycles. As the count of wet–dry cycles rises, the compressive strength of ASFS exhibits a declining pattern. After eight cycles, the compressive strength of E0Q10 dropped from 9.2 MPa to 6.9 MPa, with a reduction rate of 25%, which may be attributed to the weak interlocking ability between particles. Compared with E0Q10, the compressive strength of ASFS increased when the content of expansive soil was less than 60%. For instance, after eight cycles, the compressive strength of E6Q4 was 10% higher than that of E0Q10. This indicates that ASFS prepared with expansive soil at this dosage exhibits enhanced stability. In contrast, after eight cycles, the compressive strength of E8Q2 and E10Q0 decreased by 5.4% and 15.5%, respectively, compared with E0Q10. This indicates that excessively expansive soil may impair the structural integrity of ASFS, thereby reducing its resistance to wet–dry cycles [43,44].

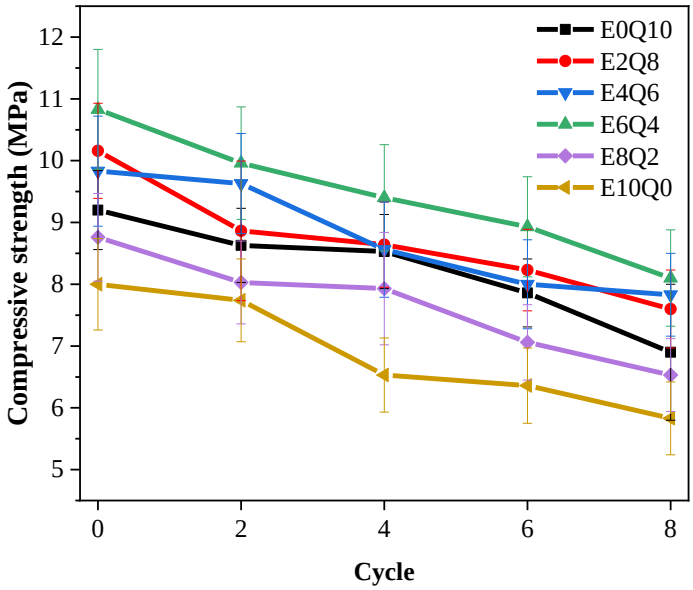

Figure 11. Compressive strength of ASFS under different numbers of wet–dry cycles.

3.8. MIP

Figure 12 presents the pore structure of ASFS with different expansive soil contents. Figure 12a shows the pore size distribution curve, E0Q10 without expansive soil exhibits a prominent peak in the large-pore range (1000–10,000 nm), indicating a very high proportion of large pores [45]. With the increase in expansive soil content, the proportion of large pores in ASFS decreases significantly, while the proportion of small pores (0–100 nm) gradually increases. This indicates that the addition of expansive soil can convert large pores into small pores through "pore size refinement", achieving the optimization of pore structure. This optimization can block the intrusion channel of external water, effectively improving the water stability of ASFS, which is also one of the reasons why ASFS prepared with expansive soil does not show significant strength reduction after immersion [42].

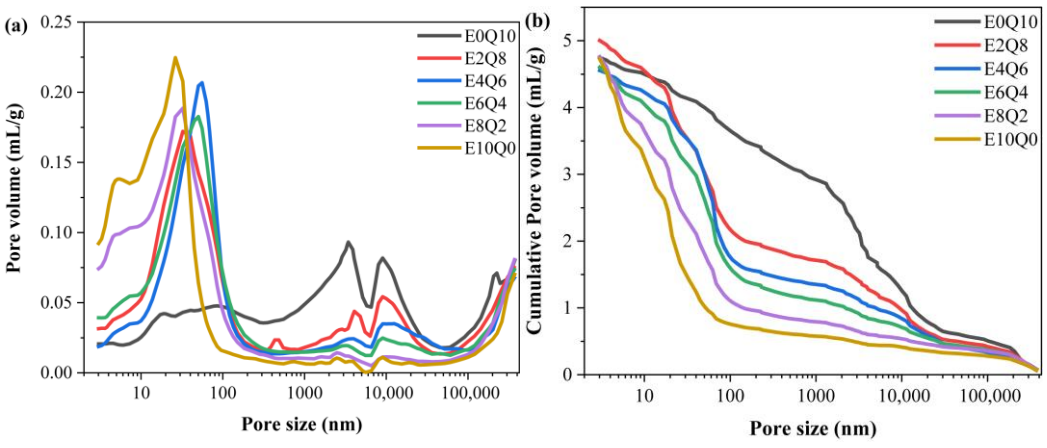

Figure 12. Pore structure of ASFS: (**a**) pore size distributions; (**b**) cumulative pore volumes.

Figure 12b presents the cumulative pore volume of ASFS. Compared with E0Q10, as the content of expansive soil was increased, the cumulative pore volume of ASFS gradually decreased with the increase in expansive soil content, indicating that expansive soil can reduce the total porosity and make the microstructure denser. This further reduces the repeated intrusion and loss of water during wet–dry cycles, enhancing the resistance to wet–dry cycles.

3.9. SEM

Figure 13 shows the SEM images of ASFS. As shown in Figure 13a, the microstructure of E0Q10 was scattered, which was related to the weak interface bonding between quartz powder and the surrounding paste of ASFS. When expansive soil was added, the microstructure of E6Q4 (Figure 13b) was significantly denser compared with E0Q10. This indicates that expansive soil, through hydration in an alkaline environment, can promote tighter bonding between quartz powder and the surrounding paste in ASFS, thereby enhancing the compressive strength of ASFS. In contrast, with the sole addition of expansive soil to ASFS, the microstructure of E10Q0 (Figure 13c) shows a blocky agglomeration morphology. This change indicates that high-content expansive soil hinders the uniform distribution of hydration products of ASFS [46].

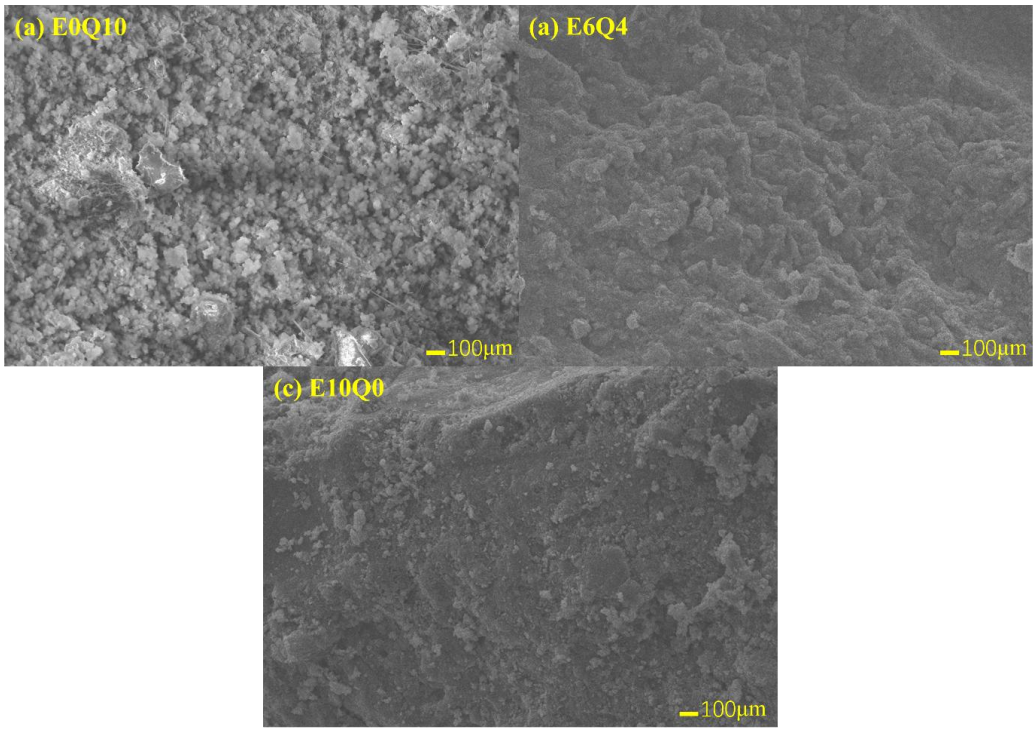

Figure 13. The typical SEM images of the samples.

4. Conclusions

This study investigated the effect of expansive soil with different content (0–100%) on ASFS and clarified the correlation laws and intrinsic action mechanisms between the dosage of expansive soil and the macroscopic properties as well as microstructure of ASFS. The following conclusions are drawn: The water absorption of expansive soil reduces the early hydration reaction rate of ASFS, and, with the increase in expansive soil dosage, the final setting time of ASFS is prolonged by 0.08–1.29 times; meanwhile, the clay minerals in expansive soil can compensate for the autogenous shrinkage of ASFS, and the reduction degree of autogenous shrinkage is proportional to the dosage of expansive soil. In addition, the optimal dosage of expansive soil in ASFS is 60%. Compared with the control group, the 7d compressive strength of ASFS is increased by 52.4%, the strength after 3-day water immersion is increased by 62.6%, and the strength after eight wet–dry cycles is still 10% higher. This result is closely related to the role of expansive soil in refining the pore structure and promoting the hydration process; however, when the dosage of expansive soil exceeds 80%, the uneven structure of ASFS is caused by particle agglomeration and insufficient hydration, which further leads to compressive strength deterioration.

5. Limitations and Implications

Although this study has achieved valuable results in optimizing the performance of ASFS by using expansive soil as an "engineering additive", there are certain limitations. Firstly, the tests were conducted under standard curing conditions (20 ± 3 °C, RH ≥ 95%), failing to fully simulate complex on-site conditions such as extreme temperature and humidity, and irregular wet–dry cycles, so the actual adaptability needs further verification. Secondly, the properties of expansive soil and slag are origin-dependent, which may restrict the promotion of the optimal 60% expansive soil dosage. Finally, this research focuses on short-term mechanical properties and short-term durability, without involving the performance evolution of ASFS under the coupled effects of repeated loads and chemical erosion during long-term service.

Nevertheless, the optimal 60% expansive soil dosage determined in this study is still of engineering value. It can increase the 7d compressive strength of ASFS by 52.4% and the 3d water immersion strength by 62.6% while compensating for autogenous shrinkage and enhancing resistance to wet–dry cycles, providing an environmentally friendly and reliable solidification scheme for subgrades and foundations of small structures in expansive soil areas. For on-site application, it is recommended to first conduct adaptability tests on local materials to calibrate the mix ratio; during construction, control the mixing uniformity, forming compactness and curing humidity. Future research can promote the standardization and large-scale application of this technology through field tests and long-term monitoring.

Author Contributions: Conceptualization, S.F. and Y.W.; methodology, Y.W. and W.T.; validation, Y.W.; investigation, Y.W., W.T., C.W., Q.W. and P.C.; resources, S.F.; data curation, Y.W.; writing—original draft preparation, Y.W. and W.T.; writing—review and editing, S.F., J.-W.W.J. and Y.T.; supervision, S.F.; funding acquisition, Y.W. All authors have read and agreed to the published version of the manuscript.

Funding: This research was funded by the Guangxi Key Research and Development Project (grant number: 2021AB17097), funded by Yongke Wei, and the Guangxi Key Research and Development Program (grant number: 2024AB24040), funded by Yongke Wei.

Data Availability Statement: The data presented in this study are available upon request from the corresponding author.

Conflicts of Interest: Author Yongke Wei is a doctoral candidate at the College of Civil Engineering, Tongji University, and also an employee of Guangxi Transportation Design Group Co., Ltd. The remaining authors declare that the research was conducted in the absence of any commercial or financial relationships that could be construed as a potential conflict of interest. The company had no role in the design of the study; in the collection, analyses, or interpretation of data; in the writing of the manuscript, or in the decision to publish the results.

References

1. Syed, M.; GuhaRay, A.; Goel, D. Strength characterisation of fiber reinforced expansive subgrade soil stabilized with alkali activated binder. *Road Mater. Pavement Des.* **2021**, *23*, 1037–1060. [CrossRef]
2. Yi, Y.; Gu, L.; Liu, S. Microstructural and mechanical properties of marine soft clay stabilized by lime-activated ground granulated blastfurnace slag. *Appl. Clay Sci.* **2015**, *103*, 71–76. [CrossRef]
3. Puppala, A.J.; Pedarla, A. Innovative ground improvement techniques for expansive soils. *Innov. Infrastruct. Solut.* **2017**, *2*, 24. [CrossRef]
4. Zha, F.; Liu, S.; Du, Y.; Cui, K. Behavior of expansive soils stabilized with fly ash. *Nat. Hazards* **2008**, *47*, 509–523. [CrossRef]
5. Woldesenbet, T.T. Experimental Study on Stabilized Expansive Soil by Blending Parts of the Soil Kilned and Powdered Glass Wastes. *Adv. Civ. Eng.* **2022**, *12*, 9645589. [CrossRef]
6. Kamei, T.; Ahmed, A.; Ugai, K. Durability of soft clay soil stabilized with recycled Bassanite and furnace cement mixtures. *Soils Found.* **2013**, *53*, 155–165. [CrossRef]

7. Puppala, A.J.; Manosuthikij, T.; Chittoori, B.C.S. Swell and shrinkage characterizations of unsaturated expansive clays from Texas. *Eng. Geol.* **2013**, *164*, 187–194. [CrossRef]
8. Daraei, A.; Herki, B.M.A.; Sherwani, A.F.H.; Zare, S. Slope Stability in Swelling Soils Using Cement Grout: A Case Study. *Int. J. Geosynth. Ground Eng.* **2018**, *4*, 10. [CrossRef]
9. Stoltz, G.; Cuisinier, O.; Masrouri, F. Weathering of a lime-treated clayey soil by drying and wetting cycles. *Eng. Geol.* **2014**, *181*, 281–289. [CrossRef]
10. Huang, K.; Xu, G.; Yan, C.; Zhang, X.; Li, D.; Cai, G.; Sun, Y.; Chen, R.; Pu, S.; Shi, X. Study on the optimization and performance of expansive soil stabilized by alkali-activated fly ash-phosphogypsum using response surface methodology. *J. Build. Eng.* **2025**, *113*, 114032. [CrossRef]
11. Li, W.; Liu, W.; Wang, B.; Zhan, X.; Zuo, J.; Shan, Y.; Han, S.; Wang, T. Synergistic effects of cement–silica fume composite on expansive soil stabilization: Mechanisms, microstructure, and durability. *Results Eng.* **2025**, *28*, 107811. [CrossRef]
12. Suhendro, B. Toward Green Concrete for Better Sustainable Environment. *Procedia Eng.* **2014**, *95*, 305–320. [CrossRef]
13. Provis, J.L.; Palomo, A.; Shi, C. Advances in understanding alkali-activated materials. *Cem. Concr. Res.* **2015**, *78*, 110–125. [CrossRef]
14. Wang, W.; Fan, C.; Wang, B.; Zhang, X.; Liu, Z. Workability, rheology, and geopolymerization of fly ash geopolymer: Role of alkali content, modulus, and water–binder ratio. *Constr. Build. Mater.* **2023**, *367*, 130357. [CrossRef]
15. Zhang, X.; Wang, B.; Chang, J. Adsorption behavior and solidification mechanism of Pb(II) on synthetic C-A-S-H gels with different Ca/Si and Al/Si ratios in high alkaline conditions. *Chem. Eng. J.* **2024**, *493*, 152344. [CrossRef]
16. Li, Z.; Chen, Y.; Provis, J.L.; Cizer, Ö.; Ye, G. Autogenous shrinkage of alkali-activated slag: A critical review. *Cem. Concr. Res.* **2023**, *172*, 107244. [CrossRef]
17. Miraki, H.; Shariatmadari, N.; Ghadir, P.; Jahandari, S.; Tao, Z.; Siddique, R. Clayey soil stabilization using alkali-activated volcanic ash and slag. *J. Rock Mech. Geotech. Eng.* **2022**, *14*, 576–591. [CrossRef]
18. Syed, M.; GuhaRay, A.; Kar, A. Stabilization of Expansive Clayey Soil with Alkali Activated Binders. *Geotech. Geol. Eng.* **2020**, *38*, 6657–6677. [CrossRef]
19. Kianynejad, M.; Toufigh, M.M.; Toufigh, V. Mechanical Performance of Alkali-activated Stabilized Sandy Soil Reinforced with Glass Wool Residue Microfibers. *KSCE J. Civ. Eng.* **2024**, *28*, 581–595. [CrossRef]
20. Yi, Y.; Li, C.; Liu, S. Alkali-Activated Ground-Granulated Blast Furnace Slag for Stabilization of Marine Soft Clay. *J. Mater. Civ. Eng.* **2015**, *27*, 04014146. [CrossRef]
21. *ASTM C191*; Standard Test Methods for Time of Setting of Hydraulic Cement by Vicat Needle. ASTM International: West Conshohocken, PA, USA, 2021.
22. *ASTM C1437*; Standard Test Method for Flow of Hydraulic Cement Mortar. ASTM International: West Conshohocken, PA, USA, 2015.
23. *ASTM C476*; Standard Specification for Grout for Masonry. ASTM International: West Conshohocken, PA, USA, 2023.
24. *ASTM C1702*; Standard Test Method for Measurement of Heat of Hydration of Hydraulic Cementitious Materials Using Isothermal Conduction Calorimetry. ASTM International: West Conshohocken, PA, USA, 2024.
25. *ASTM C1698*; Standard Test Method for Autogenous Strain of Cement Paste and Mortar. ASTM International: West Conshohocken, PA, USA, 2014.
26. Pei, C.; Chen, P.; Tan, W.; Zhou, T.; Li, J. Effect of wet copper tailings on the performance of high-performance concrete. *J. Build. Eng.* **2023**, *74*, 106931. [CrossRef]
27. *ASTM C192*; Standard Practice for Making and Curing Concrete Test Specimens in the Laboratory. ASTM International: West Conshohocken, PA, USA, 2016.
28. Parhi, P.S.; Garanayak, L.; Mahamaya, M.; Das, S.K. Stabilization of an Expansive Soil Using Alkali Activated Fly Ash Based Geopolymer. In *Advances in Characterization and Analysis of Expansive Soils and Rocks*; Hoyos, L.R., McCartney, J., Eds.; Springer International Publishing: Cham, Switzerland, 2018; pp. 36–50. [CrossRef]
29. Li, S.; Chen, D.; Jia, Z.; Li, Y.; Li, P.; Yu, B. Effects of Mud Content on the Setting Time and Mechanical Properties of Alkali-Activated Slag Mortar. *Materials* **2023**, *16*, 3355. [CrossRef]
30. Du, J.; Luo, Q.; Jiang, L.; Cao, Z.; Wang, T.; Zhang, L. Fluidized solidification modification tests on expansive soil and its mixing proportions study. *J. Zhejiang Univ. Eng. Sci.* **2024**, *58*, 2137–2148. [CrossRef]
31. Qian, J.; Hu, Y.; Zhang, J.; Xiao, W.; Ling, J. Evaluation the performance of controlled low strength material made of excess excavated soil. *J. Clean. Prod.* **2019**, *214*, 79–88. [CrossRef]
32. Chen, P.; Wang, J.; Wang, L.; Xu, Y. Perforated cenospheres: A reactive internal curing agent for alkali activated slag mortars. *Cem. Concr. Compos.* **2019**, *104*, 103351. [CrossRef]
33. Salles, F.; Douillard, J.-M.; Bildstein, O.; Gaudin, C.; Prelot, B.; Zajac, J.; Van Damme, H. Driving force for the hydration of the swelling clays: Case of montmorillonites saturated with alkaline-earth cations. *J. Colloid Interface Sci.* **2013**, *395*, 269–276. [CrossRef]

34. Srasra, E.; Bekri-Abbes, I. Bentonite clays for therapeutic purposes and biomaterial design. *Curr. Pharm. Des.* **2020**, *26*, 642–649. [CrossRef] [PubMed]
35. Zhao, H.; Ma, Y.; Zhang, J.; Hu, Z.; Li, H.; Wang, Y.; Liu, J.; Wang, K. Effect of clay content on shrinkage of cementitious materials. *Constr. Build. Mater.* **2022**, *322*, 125959. [CrossRef]
36. Ijaz, N.; Dai, F.; Meng, L.; Rehman, Z.u.; Zhang, H. Integrating lignosulphonate and hydrated lime for the amelioration of expansive soil: A sustainable waste solution. *J. Clean. Prod.* **2020**, *254*, 119985. [CrossRef]
37. Chen, Z.; Chen, P.; Li, S.; Shen, X.; Fang, J.; Gu, Z.; Wang, Y. Enhancing the performance of NaOH-activated slag using waste green tea extract as a multi-function admixture. *Case Stud. Constr. Mater.* **2024**, *21*, e03605. [CrossRef]
38. Ismail, I.; Bernal, S.A.; Provis, J.L.; Hamdan, S.; van Deventer, J.S.J. Drying-induced changes in the structure of alkali-activated pastes. *J. Mater. Sci.* **2013**, *48*, 3566–3577. [CrossRef]
39. Marsh, A.; Heath, A.; Patureau, P.; Evernden, P.; Walker, P. Influence of clay minerals and associated minerals in alkali activation of soils. *Constr. Build. Mater.* **2019**, *229*, 116816. [CrossRef]
40. Wang, W.; Lv, B.; Zhang, C.; Li, N.; Pu, S. Mechanical and micro-structure characteristics of cement-treated expansive soil admixed with nano-MgO. *Bull. Eng. Geol. Environ.* **2023**, *82*, 48. [CrossRef]
41. Ahmadi Chenarboni, H.; Hamid Lajevardi, S.; MolaAbasi, H.; Zeighami, E. The effect of zeolite and cement stabilization on the mechanical behavior of expansive soils. *Constr. Build. Mater.* **2021**, *272*, 121630. [CrossRef]
42. Shen, Q.; Wang, C.; Yan, Y.; Yi, S.; Teng, K.; Li, C. Study on Mechanism of Mechanical Property Enhancement of Expansive Soil by Alkali-Activated Slag. *Materials* **2025**, *18*, 800. [CrossRef]
43. Yang, G.; Mo, P.; Tian, Q.; Miao, Q.; Liu, D.; Pan, J. Study on Strength and Micromorphology of Expansive Soil Improved by Cement–Coal Gangue under Dry–Wet Cycle. *Adv. Civ. Eng.* **2024**, *2024*, 9976102. [CrossRef]
44. Liu, C.; Lu, K.; Wu, Z.; Liu, X.; Garg, A.; Qin, Y.; Mei, G.; Lv, C. Expansive soil improvement using industrial bagasse and low-alkali ecological cement. *Constr. Build. Mater.* **2024**, *423*, 135806. [CrossRef]
45. Han, X.; Feng, J.; Wang, B. Relationship between fractal feature and compressive strength of fly ash-cement composite cementitious materials. *Cem. Concr. Compos.* **2023**, *139*, 105052. [CrossRef]
46. Wang, H.; Liu, T.; Yan, C.; Wang, J. Expansive Soil Stabilization Using Alkali-Activated Fly Ash. *Processes* **2023**, *11*, 1550. [CrossRef]

Disclaimer/Publisher's Note: The statements, opinions and data contained in all publications are solely those of the individual author(s) and contributor(s) and not of MDPI and/or the editor(s). MDPI and/or the editor(s) disclaim responsibility for any injury to people or property resulting from any ideas, methods, instructions or products referred to in the content.